Delft University of Technology

Enhancing Wake Mixing in Wind Farms by Multi-Sine Signals in the Helix Approach

Huang, L.J.; Mulders, S.P.; Taschner, E.; Wingerden, J. W. van

Important note
To cite this publication, please use the final published version (if applicable).
Please check the document version above.

Enhancing Wake Mixing in Wind Farms by Multi-Sine Signals in the Helix Approach

L.J. Huang[1], S.P. Mulders[1], E. Taschner[1], J.W. van Wingerden[1]

Abstract— In most current offshore wind farms, the turbines are controlled greedily, neglecting any coupling by wake effects with other turbines. By neglecting these effects of aerodynamic interactions, the power production performance is substantially reduced. Besides the well-known wake steering and dynamic induction control wake control strategies, a novel wind farm flow control strategy called the Helix approach has been recently proposed to mitigate the impacts of wake effects and optimize wind farm performance. The Helix approach adopts the individual pitch control (IPC) technique to dynamically deform the wake into the helical shape, which induces wake instability and thereby stimulates wake recovery. The first results employing a single-harmonic signal have demonstrated promising enhancement in wake recovery effects. However, more complex signals to potentially improve the effectiveness of the Helix approach have never been studied. This paper explores the potential of using higher-harmonic signals in the Helix approach to further enhance wake mixing. The aeroelastic simulator, OpenFAST, with its recently developed free vortex wake codes is adopted to simulate the dynamic wake evolution. A Fourier stability analysis is used to quantitatively identify the wake breakdown position. Results show that in the baseline case where no Helix signals are implemented, the wake breaks down at 3.25 rotor diameter (D) from the rotor. When using the designed multi-sine Helix signals, the wake breaks down at 1.75 D from the rotor, which is a significant improvement over the breakdown distance at 2.50 D using the conventional single-sine Helix. The earlier wake breakdown indicates faster wake recovery and is to be validated by future higher-fidelity simulation studies.

I. INTRODUCTION

Wind turbines extract kinetic energy from the wind, and the airflow behind the turbines slows down and becomes more turbulent. These so-called wake effects result in an overall energy loss in modern wind farms of approximately 10-20% in the total energy output [1]. Moreover, wakes with a high turbulence level induce additional fatigue loads on downstream turbines, leading to premature damages on turbine components [2], reducing turbine lifetime and thereby increasing the levelized cost of electricity (LCOE).

To mitigate the impacts of wake effects and to optimize wind farm performance, a great variety of wind farm flow control strategies have been developed to ensure turbines work synergistically on a farm level (reviewed in [3]) and there is a huge momentum for sector take-up [4]. Recent efforts deploy collective pitch control (CPC) with sinusoidal control signals to excite the faster recovery of the wake so that fewer wake effects are imposed on downstream turbines [5][6][7]. However, CPC also creates a high variation
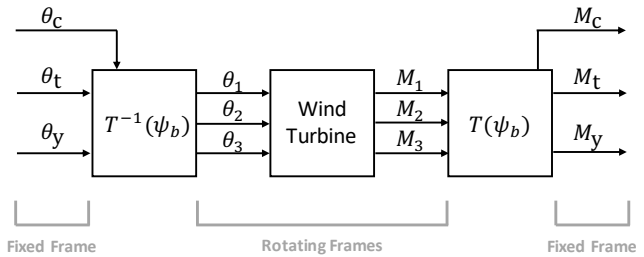
[1]Delft University of Technology, Delft Center for Systems and Control, Mekelweg 2, 2628 CD Delft, The Netherlands.

Fig. 1. The framework of the Helix approach. The individual pitch actuation signals in the rotating frames, θ_1, θ_2 and θ_3, are implemented on each blade, and these pitch perturbations are assumed to result in the amplitude-scaled and phase-shifted responses of moment signals on blade roots with the same frequency content, expressed by M_1, M_2 and M_3. The multi-blade coordinate (MBC) transformation, T, as a function of the azimuth position of each blade, ψ_b, is implemented on the moment signals to obtain the combined effects of these rotating-frame moment signals on the fixed frame, which are expressed in the tilt and yaw directions, M_t and M_y. The fixed-frame collective moment M_c is also obtained. In a similar manner, the rotating-frame pitch actuation signals can be obtained through the implementation of the inverse MBC transformation, T^{-1}, on the collective, tilt and yaw pitch actuation signals on the fixed frame, θ_c, θ_t and θ_y. The relationship between the pitch actuation signals and the moment signals on the fixed frame is obtained through the overall framework. It is noted that a nonzero presence of M_t and M_y implies that the thrust force is not acting on the rotor center. In other words, the position of the thrust force on the rotor can be dynamically manipulated by implementing the time-varying pitch actuation signals, which is considered an effective way to dynamically deflect the wake.

of power and loads on the exciting upstream turbines, adding instability in the grid [8] and causing additional damage to turbine components.

To address the aforementioned setbacks seen in CPC, the Helix approach – as proposed in [9] – takes advantage of individual pitch control (IPC) [10]. IPC is a common and well-known technique to alleviate the periodic turbine blade loads [11][12][13], where the blades are individually controlled to pitch at distinct angles. The Helix approach extends the application of IPC to the area of wind farm flow control for the first time, where IPC is exploited to deflect the wake such that wake mixing is stimulated. It is noted that the Helix approach manipulates the position of the thrust force on the rotor rather than varying its magnitude, which results in relatively constant power output and loads on the exciting upstream turbines compared with using CPC [14].

In the Helix approach framework in Fig. 1, the fixed-frame pitch actuation signals θ_t and θ_y lead to different ways of manipulating thrust force, and thereby resulting in a varying extent of wake mixing. In the previous work of the Helix approach, the pitch actuation signals are constrained to a

sinusoid at a fixed amplitude and frequency. However, the study of adopting higher harmonic signals to achieve better wake mixing has never been conducted.

This paper presents the results of employing designed multi-sine pitch actuation signals in the Helix approach towards further enhanced wake mixing compared to the traditional single-sine signals. Simulations are performed in the framework of OpenFAST [15], and the wake dynamics are modeled through the free vortex wake (FVW) method. The FVW method is preferred in this study due to its capability to capture complex vortex evolution in the wake development and its substantially lower computational costs than the traditional CFD modeling tools. The wake mixing process is quantitatively analyzed by the Fourier stability analysis. The IEA 10-MW reference wind turbine is employed, subject to a steady and uniform wind profile with a mean wind speed of 10 m/s. The contributions of the paper are as follows:

1) Proposing a framework for synthesizing multi-sine pitch actuation signals in the Helix approach to effectively achieve earlier wake breakdown.
2) Showing the results of higher-harmonic pitch actuation signals in the Helix approach for the first time.
3) Formalizing an analysis framework for evaluating the effectiveness of proposed control signals quantifying the wake breakdown position.
4) Providing insights for future optimization of advanced pitch actuation signals.

II. THEORY OF THE HELIX APPROACH

This section presents the theories used for the Helix approach. First, Section II-A describes how the MBC transformation is employed in the Helix framework. Then, Section II-B outlines how the thrust force and consequently the wake is manipulated by IPC. Last, the design of actuation signals is discussed in Section II-C.

A. The MBC transformation for three-bladed turbines

In a multi-bladed rotor system, blade dynamics are often expressed in the rotating frames attached to themselves. However, it is of great interest to also understand the coupled effects of these quantities expressed in the fixed frame of the rotor. For example, the rotor and the tower-nacelle subsystem always see and respond to the effects of the blades as a whole instead of individually. Therefore, the forward and inverse MBC transformations, which are also referred to as the Fourier coordinate transformations or the Coleman transformations, are introduced as mathematical tools to project the rotating frames in the fixed frame, and vice versa. The MBC transformation was first used in the field of helicopter theory where the rotor dynamics are of interest, and it was later widely applied to the field of wind turbines [16]. In the remainder of this section, the formulas of the forward and inverse MBC transformations are presented, which is according to Johnson's work [17].

Consider a rotor with N blades equidistantly located. Then the azimuth of the bth blade is defined as

$$\psi_b = \psi + (b-1)\frac{2\pi}{N}. \tag{1}$$

It is assumed that ψ is zero when the first blade is vertically pointing up and increases in the clockwise direction, where $\{\psi \in \mathbb{R} : 0 \leq \psi < 2\pi\}$.

Let q_b be a certain quantity on the bth rotating blade, which is a function of ψ_b. For each blade at different ψ_b, q_b has a different effect on the overall rotor plane. To combine these individual effects into an overall effect, the forward MBC transformation is expressed by the following respective collective, n-cosine-cyclic and n-sine-cyclic contributions in the fixed frame:

$$q_{\text{c}} = \frac{1}{N}\sum_{b=1}^{N} q_b, \tag{2}$$

$$q_{\text{nc}} = \frac{2}{N}\sum_{b=1}^{N} q_b \cos(n\psi_b), \tag{3}$$

$$q_{\text{nc}} = \frac{2}{N}\sum_{b=1}^{N} q_b \sin(n\psi_b), \tag{4}$$

with n being the harmonic index.

For a three-bladed turbine system ($N = 3$), the matrix form of the forward MBC transformation

$$\begin{bmatrix} M_{\text{c}} \\ M_{\text{t}} \\ M_{\text{y}} \end{bmatrix} = T(\psi) \begin{bmatrix} M_1 \\ M_2 \\ M_3 \end{bmatrix}, \tag{5}$$

with harmonic index $n = 1$ is implemented on moment signals, and is therefore expressed by:

$$T(\psi) = \frac{2}{3} \begin{bmatrix} 1/2 & 1/2 & 1/2 \\ \cos(\psi_1) & \cos(\psi_2) & \cos(\psi_3) \\ \sin(\psi_1) & \sin(\psi_2) & \sin(\psi_3) \end{bmatrix}. \tag{6}$$

By doing so, the individual moments on blade roots are combined and re-expressed in the tilt and the yaw directions. Moreover, the collective moment is calculated, which indicates the overall magnitude of the moment relative to the center of the rotor.

Similarly, the matrix form of the inverse MBC transformation

$$\begin{bmatrix} \theta_1 \\ \theta_2 \\ \theta_3 \end{bmatrix} = T^{-1}(\psi) \begin{bmatrix} \theta_{\text{c}} \\ \theta_{\text{t}} \\ \theta_{\text{y}} \end{bmatrix}, \tag{7}$$

acts on the fixed-frame pitch actuation signals as expressed by

$$T^{-1}(\psi) = \begin{bmatrix} 1 & \cos(\psi_1) & \sin(\psi_1) \\ 1 & \cos(\psi_2) & \sin(\psi_2) \\ 1 & \cos(\psi_3) & \sin(\psi_3) \end{bmatrix}. \tag{8}$$

Through the implementation of the forward and inverse MBC transformations in the framework seen in Fig. 1, the pitch actuation signals and the blade-root moment signals are linked, where these signals are both expressed in the tilt and the yaw directions in the fixed frame.
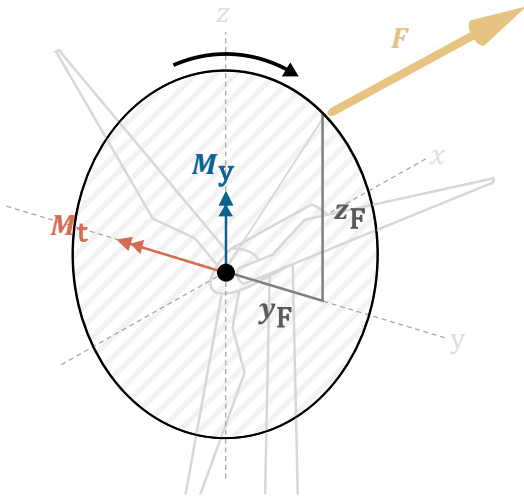
Fig. 2. The illustration of the thrust force manipulation in the Helix approach. The fixed-frame pitch actuation signals θ_t and θ_y are implemented and induce the corresponding fixed-frame moments M_t and M_y on the rotor. The distance between the thrust force F and the rotor center is defined by italics y_F and z_F. The black line represents the trajectory of the thrust force. By implementing specific combinations of θ_t and θ_y, the position of the thrust force is dynamically manipulated, which aims to result in wake deflection and thereby enhancing wake mixing. It is noted that the shown trajectory of the thrust force position is enlarged for the purpose of illustration.

B. Thrust force and wake manipulation

The occurrence of the tilt and the yaw moments implies that the thrust force is not acting on the center of the rotor. Specifically speaking, when the blades are pitched individually, each blade may experience a different aerodynamic force distribution. The overall thrust force exerted on the rotor can move away from the center of the rotor, creating the tilt and yaw moments with respect to the rotor center. Since the thrust force is the overall axial force the rotor exerts on the wind flow, forming the wake behind the rotor, the deflection of the wake can therefore be induced by the dynamic manipulation of thrust-force position.

As shown in Fig. 2, the thrust force position on the rotor is defined by the horizontal and the vertical coordinate distance between the thrust force and the rotor center, respectively indicated by y_F and z_F. The distances y_F and z_F are defined by

$$y_F = \frac{M_y}{F}, \qquad (9)$$

$$z_F = -\frac{M_t}{F}, \qquad (10)$$

dividing the yaw and the tilt moments by the thrust force with the magnitude of F. It is noted that the negative sign in z_F is introduced for the purpose of being consistent with the conventional notation of moments.

C. Design of pitch actuation signals

The combinations of θ_t and θ_y determine the thrust-force trajectory, which eventually affects the wake development. In this paper, two designed combinations are introduced.

1) Single-sine design: Both θ_t and θ_y are constrained in being a single-frequency sinusoid in their general form as

$$\theta_t = \bar{\theta}_t \sin\left(f_e t\right), \qquad (11)$$

$$\theta_y = \bar{\theta}_y \sin\left(f_e t + \Phi\right), \qquad (12)$$

where $\bar{\theta}_t$ and $\bar{\theta}_y$ are amplitudes of the tilt and yaw pitch actuation signals, f_e is the excitation frequency, t is the current time, and Φ is the phase lead by θ_t from θ_y.

2) Multi-sine design: A multi-sine signal is composed of multiple sinusoidal signals given with their excitation frequencies, amplitudes, and phases, and this extends the flexibility to design the more advanced pitch actuation signals in the Helix approach. In this paper, the designed form of multi-sine signals is given by

$$\theta_t = \bar{\theta}_t[a + \cos\left(rf_e t\right)] \sin\left(f_e t\right), \qquad (13)$$

$$\theta_y = \bar{\theta}_y[a + \cos\left(rf_e t\right)] \sin\left(f_e t + \Phi\right), \qquad (14)$$

where a is a constant and r is the multiple integer of excitation frequencies. The multi-sine signals are designed to have periodically changing amplitudes of pitch actuation, which aims to induce the instability of the tip vortices during the wake development.

III. METHODOLOGY

This section presents the methods adopted to perform the simulation work in this paper. First, the setup of the simulation environment is introduced in Section III-A. Then, the specification of the simulation cases is explained in Section III-B. Last, the Fourier stability analysis which is used to analyze the results is discussed in Section III-C.

A. Wind turbine and wake simulation environment

The dynamic aero-servo-elastic wind turbine simulations are performed using OpenFAST. The IEA 10-MW reference wind turbine is used for the case study where its Open-FAST definition can be found in [18]. The reference open-source controller (ROSCO) [19] is employed as the turbine controller. The source codes of ROSCO are modified to include the individual pitch actuation enabling the (multi-sine) Helix approach. The wind speed is set to a mean wind speed of 10 m/s, in an orientation perpendicular to the rotor plane for all the simulation cases. No turbulence, wind shear, and yaw misalignment are considered. The free vortex wake (FVW) aerodynamic module of OpenFAST, named after cOnvecting LAgrangian Filaments (OLAF) [20], is employed to capture the wake development dynamics. The FVW method is adopted since it is less computationally costly than conventional high-fidelity CFD models by orders of magnitude [21], and it has been widely applied in the field of wind turbine research to analyze the vortex stability in the wake development [22][23][24].

B. Simulation cases

Three simulation cases are studied in this paper: baseline (BL), single-sine (SS), and multi-sine (MS). The parameters of pitch actuation signals for these cases corresponding to $(11)-(14)$ are listed in Tab. I.

It is noted that f_e is characterized by the dimensionless Strouhal number (St) defined as $St = f_e D/U$, where D is the rotor diameter and U is the free-stream wind speed. To be consistent with the frequency used in the previous work of the Helix approach [9], St of 0.25 is adopted which corresponds to $f_e = 0.011$ Hz at a wind speed of 10 m/s and with the rotor diameter of 198 m. The chosen f_e is around one order of magnitude slower than the wind turbine's rotational speed.

The constants a and r as in (13) and (14) used for MS are determined as an initial choice and have not been optimized, but the combination already demonstrates promising improvement in the wake mixing which is discussed in the latter sections.

TABLE I
PARAMETERS OF PITCH ACTUATION SIGNALS FOR SIMULATION CASES.

Case Name	$\bar{\theta}_t$ [deg]	$\bar{\theta}_y$ [deg]	f_e [Hz]	Φ [deg]	a [-]	r [-]
BL	-	-	-	-	-	-
SS	4	4	0.011	90	-	-
MS	5.8	5.8	0.011	90	0.05	0.95

To ensure the actuator duty cycle (ADC) [25] on the pitch bearings are at the same level, the SS and MM cases are designed to attain a similar level by calibrating the amplitudes of actuation signals. The ADC is defined by

$$\text{ADC} = \frac{1}{T_\theta} \int_{t=0}^{T_\theta} \frac{\beta(t)}{\beta_{\max}} \mathrm{d}t, \tag{15}$$

where T_θ is the period of the pitch activities, $\beta(t)$ is the pitch rate at the given time of t, and $\beta_{\max}$ is the maximum pitch rate.

C. Fourier stability analysis

In the Helix approach, the periodic individual actuation induces instability of the wake and thereby stimulates the wake breakdown. To quantify the wake breakdown process, Fourier stability analysis is employed.

The velocity profiles downstream of the turbine are expressed as $u_{j,x}$, where u is the time-series velocity data collected at the location represented by x and j, x indicates the downstream distance from the rotor center, and j indicates the position of the point on the given downstream cross-section. Each velocity profile, $u_{j,x}$, is composed of M snapshots taken equidistantly during a time period, and is transformed from the time domain to the frequency domain by the Fourier transform defined by

$$\hat{u}_{j,x} = \frac{1}{M} \sum_{m=0}^{M-1} u_{j,x} \, e^{-2\pi \mathrm{i}\left(\frac{mk}{N}\right)} \tag{16}$$

where $\hat{u}_{j,x}$ is the Fourier coefficient as a function of k, m is the index of the snapshot, i is the imaginary unit, and k is the frequency mode.

The absolute value of the Fourier coefficient, $|\hat{u}_{j,x}|$, represents the amplitude of the perturbation, so tracking $|\hat{u}_{j,x}|$ along the rotor axis can depict the growth of the instability. To achieve this, the maximum absolute value of $|\hat{u}_{j,x}|$ including all the frequency modes on each cross-section, is defined by

$$\hat{u}_x^{\max} = \max\left(|\hat{u}_{j,x}|\right). \tag{17}$$

The growth of the amplitude follows the form of the exponential function when the mutual induction between the vortices, known as vortex-pairing, begins [26][27]. This process is expressed by

$$\frac{\hat{u}_{x=x_2}^{\max}}{\hat{u}_{x=x_1}^{\max}} = e^{\sigma(x_2-x_1)/U}, \tag{18}$$

where σ is the instability growth rate, x_1 and x_2 are the given stream-wise positions. When the vortical structure fully breaks down, the amplitude starts to saturate and stops growing.

IV. RESULTS

This section presents the simulation results. First, the projected moments and their effect on the thrust force are shown in Section IV-A. Next, the wake development characterized by tip and root vortices is demonstrated in Section IV-B. Lastly, the Fourier analysis used to quantify the wake breakdown process is discussed in Section IV-C.

A. Thrust force manipulation

Individual pitch actions are implemented on the blades according to the actuation signals specified in Tab. I. Due to the dynamic change of the blade pitch angles, the aerodynamic loads along each of the blades vary with time, which induces dynamic moments on the blade roots. The blade-root moments of three blades are projected on the fixed frame by the MBC transformation, and the combined effect can be expressed by M_c, M_t and M_y, as shown in Fig. 3. For SS, sinusoidal signals are used, where the tilt signal (orange line) leads the yaw signal (blue line) by $\pi/2$. The excitation frequency is taken as $f_e = 0.011$ Hz results in the actuation period of around 90 seconds. It is noted that the M_c remains constant, indicating that the overall thrust force magnitude
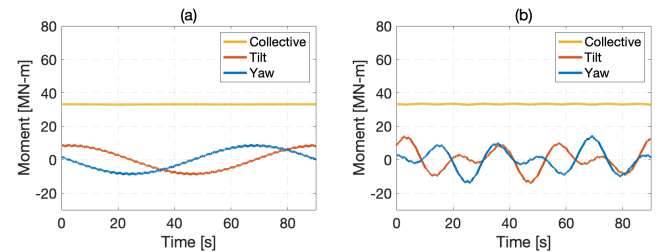

Fig. 3. Moment signals in the fixed frame for simulation cases of (a) SS (b) MS. The collective, tilt, and yaw moments are represented by the yellow, orange and blue line, respectively.
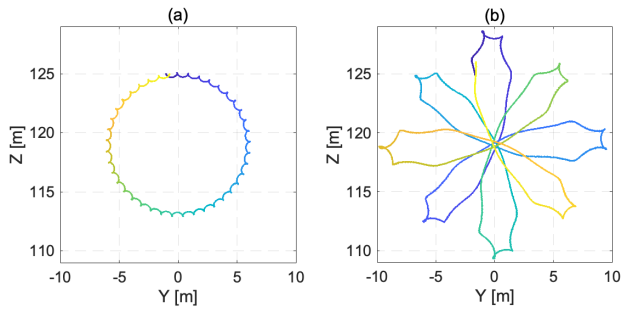
Fig. 4. The trajectory of the thrust force position seen from the front view on the rotor plane for simulation cases of (a) SS (b) MS. The Y and Z are the horizontal and the vertical coordinate, respectively, representing the rotor plane. The trajectory is represented by the color from blue to yellow with respect to the simulation time from the beginning to the end.
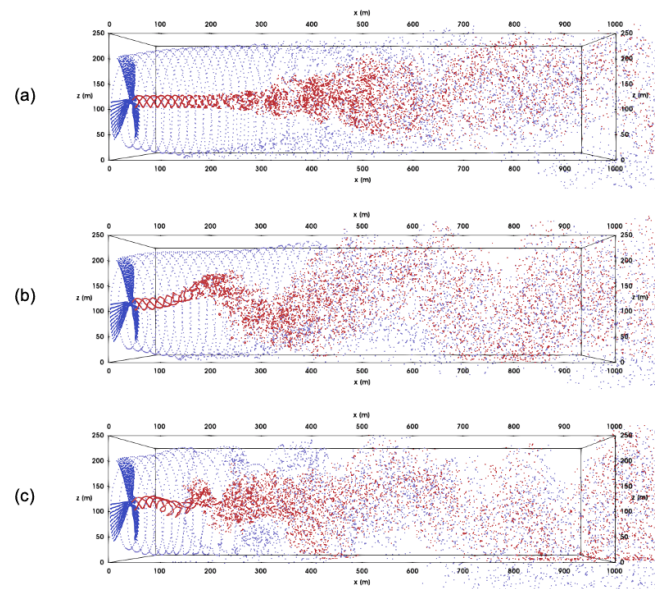

Fig. 5. The instantaneous capture of the vortex evolution within 5D downstream of the turbine for simulation cases of (a) BL (b) SS and (c) MS. The simulation is performed in OpenFAST with the OLAF aerodynamic module. The vortices are generated and emitted from the lifting lines which represent the blades. In the wake region of $30°$ span close to the blades, the vortex lattice representation is adopted, where the vortices on along the whole blade are captured. These vortices are represented by the blue particles. After this region, the wake is assumed to roll up into the tip and the root vortices, which are represented by the blue and the red particles, respectively.

experienced by the rotor is constant. For MS, the design of periodic amplitudes in (13) and (14) induce more complex moments with higher harmonics. The M_c is still kept at a relatively constant level.

According to the tilt and the yaw moments, the trajectory of the thrust force acting on the rotor is determined, as illustrated in Fig. 4. For SS, the thrust force deviates from the center of the rotor by around 5 meters, and rotates circularly around the rotor center in the clockwise direction. For MS, the trajectory of the thrust force is more complex and is explained in the following. Starting from the location of around $(X, Y) = (0, 130)$, the thrust force passes through the rotor center of $(X, Y) = (0, 119)$ and moves to the location of around $(X, Y) = (-5, 113)$. The same process repeats over and over again, resulting in the trajectory of the shape of a flower with eight petals in the clockwise direction.

B. Wake development

The dynamic thrust force manipulates the wake formation, which is exploited to stimulate the wake breakdown process and thereby enhances wake mixing. The wake breakdown process can be visualized by tracking the evolution of the tip and root vortices, as shown in Fig. 5. The mutual induction between tip vortices, known as vortex pairing, drives the breakdown of the wake, which is the triggering event for the onset of wake mixing [28]. After the tip vortical structure vanishes, the re-energizing process starts. In this region, the wake recovers its kinetic energy by turbulent mixing with the ambient air.

For BL, the thrust force is acting on the rotor center, so the wake is steadily formed and aligns with the inflow wind direction. For SS, the thrust force position rotates around the rotor center, which leads to the helical downstream wake formation and thereby fosters the wake breakdown. For MS, the thrust force position moves closer to and further away from the rotor center periodically in the flower shape. By doing so, the boundary of the wake is periodically perturbed, which induces the instability of the tip vortical structures. This perturbation is considered to provide the driving force to

trigger the breakdown of the tip vortical structure. Therefore, the wake starts mixing even earlier than in the case of SS.

The velocity field behind the rotor at the distance of 1 rotor diameter (D) from the front view is shown in Fig. 6. The velocity field is captured every 11 seconds for overall one period of the actuation in the Helix approach. For SS, it is observed that the wake is deflected from the rotor region projected at 1D downstream distance, and rotates in the clockwise direction with time. For MS, there is no clear rotation of the wake observed since the thrust manipulation is more complex. It is noted that the boundary of the wake becomes blurred with the ambient flow, and it is an important indication that the tip vortical structure already starts to break down in the early stage.

C. Fourier stability analysis

The Fourier stability analysis is exploited to provide a more quantitative aspect in comparing the wake breakdown process. At each dimensionless downstream distance (x/D), the maximum absolute value of the Fourier coefficient represents the amplitude of the perturbation at that location, which is regarded as the indicator of instability. By tracking the amplitude of the perturbation along the downstream distance, the instability growth and the wake breakdown location can be identified.

Fig. 7 shows the instability growth along the dimensionless downstream distance. In the semi-logarithmic plot, the linear trend refers to the exponential change of the value, and
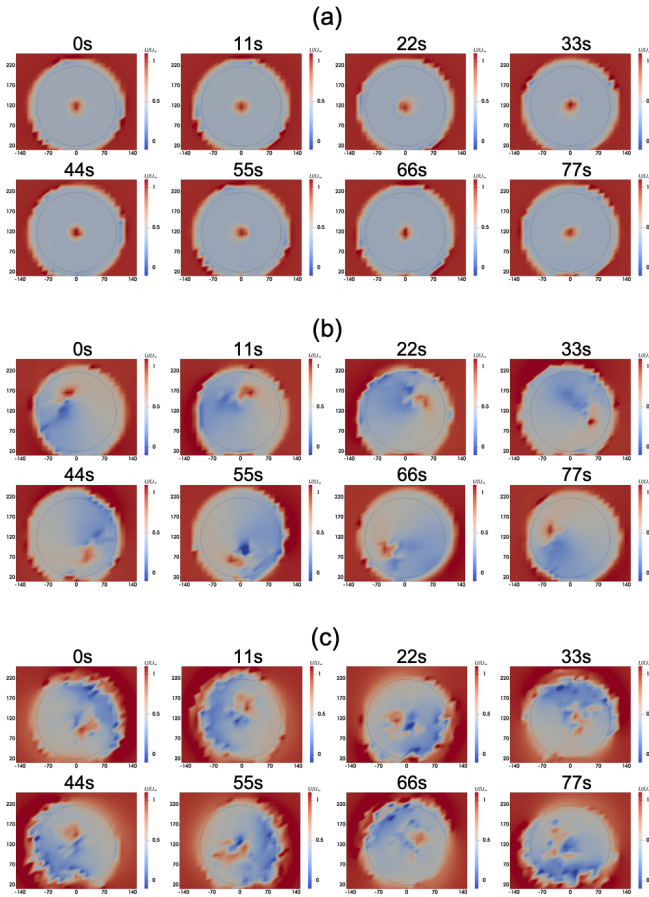
828

Fig. 6. The normalized velocity field behind the rotor at the distance of 1D seen from the front view at different time instances for simulation cases of (a) BL (b) SS and (c) MS. The horizontal and vertical dimensions are expressed in the unit of meters. The red area represents higher wind velocity and the black circle represents the rotor region projected on the 1D plane.
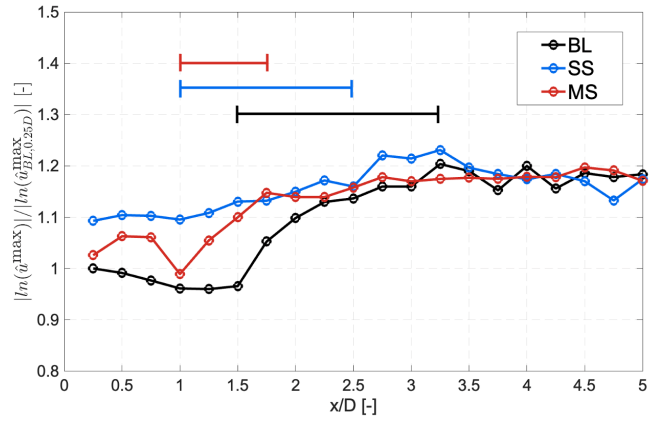

Fig. 7. The instability growth along the dimensionless downstream distance. The vertical axis is the maximum absolute Fourier coefficient in the logarithmic scale normalized by the value in the case of BL at 0.25 D. The top lines represent the instability linear growth (vortex-pairing) region.

this is regarded as the instability growth caused by the vortex-pairing. The instability continues growing until the wake fully breaks down and enters the wake-mixing process. Therefore, the location where the instability starts to saturate implies the location where the wake fully breaks down. By doing so, the effectiveness of the actuation signals on wake development can be compared by identifying the wake breakdown locations.

For BL, the linear instability growth starts at 1.5 D and ends at 3.25 D. It means that the vortex pairing starts at 1.5 D, and the instability is growing until the vortices break down at 3.25 D. In other words, the downstream distance of 3.25 D can be regarded as the location where the wake fully breaks down. Similarly, the wake breakdown position of SS and MS is 2.50 D and 1.75 D, respectively. The results of the Fourier stability analysis show that MS enhances in stimulating the wake breakdown process over SS.

V. CONCLUSIONS

The Helix approach is a state-of-art wind farm control strategy that exploits individual pitch control (IPC) to enhance wind farm performance by stimulating wake recovery.

In previous work on the Helix approach, single-sine pitch actuation signals were employed, but the inclusion of higher-harmonic actuation signals has never been studied.

This paper has shown the first results of synthesizing and implementing multi-sine signals in the Helix approach. The IEA 10-MW reference turbine operating in the steady and uniform wind at a speed of 10 m/s is simulated in the framework of OpenFAST. The free vortex wake method is used to simulate the dynamics of the wake development. A Fourier stability analysis framework has been derived to quantitatively identify the wake breakdown location.

Three simulation cases are provided in this paper: baseline (BL), single-sine (SS), and multi-sine (MS). The results have shown that the wake breakdown location at the downstream distance of BL, SS, and MS is 3.25 D, 2.50 D, and 1.75 D, respectively. The SS and MS cases are designed in such a way that the same actuator duty cycle (ADC) load level is attained. Therefore, two key findings can be interpreted from the results: (1) implementing the traditional single-sine pitch actuation signals can already induce earlier wake breakdown than the baseline by 0.75–1.00 D, and (2) implementing the proposed multi-sine pitch actuation signals can additionally achieve earlier wake breakdown by 0.75 D. The earlier wake breakdown is considered to result in the earlier onset of the wake mixing process.

Therefore, it is concluded that implementing the proposed multi-sine pitch actuation signals induces the earlier breakdown of the tip vortices which prevents wake mixing, and thereby has the potential to provide additional enhancements for Helix-based wake mixing control strategies.

VI. FUTURE WORK

The recommendations to solve the open challenges in future work are described below:

1) The main limitation of this study is that the multi-sine Helix approach is only investigated in the uniform and steady inflow conditions. The effectiveness of

the proposed approach has not been verified for non-idealized inflow conditions considering turbulence and wind shear. In the context of applying a realistic wind atmospheric boundary layer, the wake can breakdown much earlier without blade perturbation, so the physics exploited in the proposed approach to accelerate the wake breakdown process can possibly be less effective. Therefore, studies considering realistic inflow conditions are recommended for future work.

2) The amount of wind velocity recovery using the multi-sine Helix approach has not been investigated. Although the FVW method has the advantage of simulating vortex dynamics at less computational costs, it has the limitation in predicting wind fields in the wake mixing region [22]. Therefore, it is recommended to perform higher-fidelity CFD modeling such as large-eddy simulations to investigate the dynamics in the far wake region, and to understand the additional energy that could be recovered by implementing the multi-sine Helix approach.

REFERENCES

[1] R. J. Barthelmie, K. Hansen, S. T. Frandsen, O. Rathmann, J. Schepers, W. Schlez, J. Phillips, K. Rados, A. Zervos, E. Politis, *et al.*, "Modelling and measuring flow and wind turbine wakes in large wind farms offshore," *Wind Energy: An International Journal for Progress and Applications in Wind Power Conversion Technology*, vol. 12, no. 5, pp. 431–444, 2009.

[2] J. F. Manwell, J. G. McGowan, and A. L. Rogers, *Wind energy explained: theory, design and application*. John Wiley & Sons, 2010.

[3] J. Meyers, C. Bottasso, K. Dykes, P. Fleming, P. Gebraad, G. Giebel, T. Göçmen, and J. van Wingerden, "Wind farm flow control: prospects and challenges," *Wind Energy Science*, vol. 7, no. 6, pp. 2271–2306, 2022. [Online]. Available: https://wes.copernicus.org/articles/7/2271/2022/

[4] J. W. van Wingerden, P. A. Fleming, T. Göçmen, I. Eguinoa, B. M. Doekemeijer, K. Dykes, M. Lawson, E. Simley, J. King, D. Astrain, M. Iribas, C. L. Bottasso, J. Meyers, S. Raach, K. Kölle, and G. Giebel, "Expert elicitation on wind farm control," *Journal of Physics: Conference Series*, vol. 1618, no. 2, p. 022025, sep 2020. [Online]. Available: https://dx.doi.org/10.1088/1742-6596/1618/2/022025

[5] W. Munters and J. Meyers, "Towards practical dynamic induction control of wind farms: analysis of optimally controlled wind-farm boundary layers and sinusoidal induction control of first-row turbines," *Wind Energy Science*, vol. 3, no. 1, pp. 409–425, 2018.

[6] J. A. Frederik, R. Weber, S. Cacciola, F. Campagnolo, A. Croce, C. Bottasso, and J. W. van Wingerden, "Periodic dynamic induction control of wind farms: proving the potential in simulations and wind tunnel experiments," *Wind Energy Science*, vol. 5, no. 1, pp. 245–257, 2020.

[7] D. van der Hoek, J. Frederik, M. Huang, F. Scarano, C. Simao Ferreira, and J. W. van Wingerden, "Experimental analysis of the effect of dynamic induction control on a wind turbine wake," *Wind Energy Science*, vol. 7, no. 3, pp. 1305–1320, 2022. [Online]. Available: https://wes.copernicus.org/articles/7/1305/2022/

[8] S. Muyeen and A. Al-Durra, *Modeling and control aspects of wind power systems*. BoD–Books on Demand, 2013.

[9] J. A. Frederik, B. M. Doekemeijer, S. P. Mulders, and J. W. van Wingerden, "The helix approach: Using dynamic individual pitch control to enhance wake mixing in wind farms," *Wind Energy*, vol. 23, no. 8, pp. 1739–1751, 2020.

[10] S. P. Mulders, A. K. Pamososuryo, G. E. Disario, and J. W. v. Wingerden, "Analysis and optimal individual pitch control decoupling by inclusion of an azimuth offset in the multiblade coordinate transformation," *Wind Energy*, vol. 22, no. 3, pp. 341–359, 2019. [Online]. Available: https://onlinelibrary.wiley.com/doi/abs/10.1002/we.2289

[11] S. T. Navalkar, J. W. van Wingerden, E. van Solingen, T. Oomen, E. Pasterkamp, and G. Van Kuik, "Subspace predictive repetitive control to mitigate periodic loads on large scale wind turbines," *Mechatronics*, vol. 24, no. 8, pp. 916–925, 2014.

[12] S. T. Navalkar, E. van Solingen, and J. W. van Wingerden, "Wind tunnel testing of subspace predictive repetitive control for variable pitch wind turbines," *IEEE Transactions on Control Systems Technology*, vol. 23, no. 6, pp. 2101–2116, 2015.

[13] J. Frederik, L. Kröger, G. Gülker, and J. W. van Wingerden, "Data-driven repetitive control: Wind tunnel experiments under turbulent conditions," *Control Engineering Practice*, vol. 80, pp. 105–115, 2018.

[14] J. A. Frederik and J. W. van Wingerden, "On the load impact of dynamic wind farm wake mixing strategies," *Renewable Energy*, vol. 194, pp. 582–595, 2022. [Online]. Available: https://www.sciencedirect.com/science/article/pii/S0960148122007613

[15] N. R. E. Laboratory. Openfast documentation. [Online]. Available: https://openfast.readthedocs.io/en/main/index.html

[16] G. Bir, "Multi-blade coordinate transformation and its application to wind turbine analysis," in *46th AIAA aerospace sciences meeting and exhibit*, 2008, p. 1300.

[17] W. Johnson, *Rotorcraft aeromechanics*. Cambridge University Press, 2013, vol. 36.

[18] P. Bortolotti, H. C. Tarres, K. Dykes, K. Merz, L. Sethuraman, D. Verelst, and F. Zahle, "IEA wind task 37 on systems engineering in wind energy – wp2.1 reference wind turbines," NREL/TP-73492, International Energy Agency, Tech. Rep., 2019. [Online]. Available: https://www.nrel.gov/docs/fy19osti/73492.pdf

[19] P. Bortolotti, K. Dykes, K. Merz, and F. Zahle, "IEA wind task 37 on systems engineering in wind energy," *WP2-Reference Wind Turbines.: IEA Wind Task*, vol. 37, 2019.

[20] K. Shaler, E. Branlard, and A. Platt, "OLAF user's guide and theory manual," National Renewable Energy Lab.(NREL), Golden, CO (United States), Tech. Rep., 2020.

[21] M. Tugnoli, D. Montagnani, M. Syal, G. Droandi, and A. Zanotti, "Mid-fidelity approach to aerodynamic simulations of unconventional vtol aircraft configurations," *Aerospace Science and Technology*, vol. 115, p. 106804, 2021.

[22] D. Marten, C. O. Paschereit, X. Huang, M. Meinke, W. Schroeder, J. Mueller, and K. Oberleithner, "Predicting wind turbine wake breakdown using a free vortex wake code," *AIAA Journal*, vol. 58, no. 11, pp. 4672–4685, 2020.

[23] S. N. Rodriguez, J. W. Jaworski, and J. G. Michopoulos, "Stability of helical vortex structures shed from flexible rotors," *Journal of Fluids and Structures*, vol. 104, p. 103279, 2021.

[24] K. Brown, D. Houck, D. Maniaci, C. Westergaard, and C. Kelley, "Accelerated wind-turbine wake recovery through actuation of the tip-vortex instability," *AIAA Journal*, vol. 60, no. 5, pp. 3298–3310, 2022.

[25] C. L. Bottasso, F. Campagnolo, A. Croce, and C. Tibaldi, "Optimization-based study of bend–twist coupled rotor blades for passive and integrated passive/active load alleviation," *Wind Energy*, vol. 16, no. 8, pp. 1149–1166, 2013.

[26] S. Ivanell, R. Mikkelsen, J. N. Sørensen, and D. Henningson, "Stability analysis of the tip vortices of a wind turbine," *Wind Energy*, vol. 13, no. 8, pp. 705–715, 2010.

[27] S. Sarmast, R. Dadfar, R. F. Mikkelsen, P. Schlatter, S. Ivanell, J. N. Sørensen, and D. S. Henningson, "Mutual inductance instability of the tip vortices behind a wind turbine," *Journal of Fluid Mechanics*, vol. 755, pp. 705–731, 2014.

[28] L. Lignarolo, D. Ragni, F. Scarano, C. S. Ferreira, and G. Van Bussel, "Tip-vortex instability and turbulent mixing in wind-turbine wakes," *Journal of Fluid Mechanics*, vol. 781, pp. 467–493, 2015.